19

# Electrically small resonators for metamaterial and microwave circuit design

Marta Gil, Francisco Aznar, Adolfo Vélez,
Miguel Durán-Sindreu, Jordi Selga, Gerard Sisó,
Jordi Bonache and Ferran Martín
*Universitat Autònoma de Barcelona (GEMMA/CIMITEC Group)*
*Spain*

## 1. Introduction

A new branch in microwave engineering arose just few years ago with the emergence of metamaterials in 2000 (Smith et al., 2000). The implementation of the first artificial medium with negative effective dielectric permittivity and magnetic permeability opened the door to the experimental study of a new kind of media: left-handed media. The possibility of the artificial implementation of such media allowed the corroboration of many of their electromagnetic properties, predicted years before by Viktor Veselago (Veselago, 1968). Since the year 2000, the interest stirred up by these new materials has given rise to numerous works in a wide range of scientific branches. The possibilities that metamaterials offer to create artificial media with controllable characteristics has permitted the creation of a growing number of completely new applications. Undoubtedly, the most innovative and spectacular application of such artificial media is their use in the implementation of cloaking structures to achieve invisibility, which can be accomplished thanks to the engineering of the refraction index of the different layers of the cloaking shield (Schurig et al., 2006). Within the vast number of new applications of metamaterials, one of the most productive ones is the implementation of microwave devices by means of artificial transmission lines. The following sections will deal with one of the approaches devoted to this purpose: the resonant-type approach. Different subwavelength resonators employed in the design of metamaterial transmission lines based on the resonant-type approach will be studied. The equivalent circuit models of different kinds of metamaterial transmission lines, as well as the parameter extraction methods employed as design and corroboration tools will be also presented. In closing, a selection of application examples of resonant-type metamaterial transmission lines in the design of microwave devices will be presented.

## 2. Sub-wavelength resonators

The implementation of the first effective medium with left handed properties (Smith et al., 2000) was possible thanks to the employment of small metallic resonators known as split-ring resonators (SRRs). These resonators had been previously presented (Pendry et al., 1999) as the first non-magnetic resonator capable of exhibiting negative values of the magnetic permeability around its resonance frequency. This was one of the characteristics which made the SRR suitable for the synthesis of such a medium; the second one was its small electrical size. At the resonance frequency, the SRR perimeter is smaller than half the wavelength of the exciting wave. These small dimensions allow the use of SRRs in the implementation of effective media, which requires small unit cell sizes (smaller than the wavelength). By this means, the incident radiation does not detect the internal configuration of the medium, but the effective properties of the whole medium.
The split-ring resonator is formed by two concentric metallic open rings (see Fig.1). The resonator can be excited by an axial (z direction in the figure) time-varying external magnetic field, which induces currents in the rings. The splits present in the rings force the current to flow as displacement current between them. The current loop is thus closed through the distributed capacitance that appears between the inner and the outer ring.

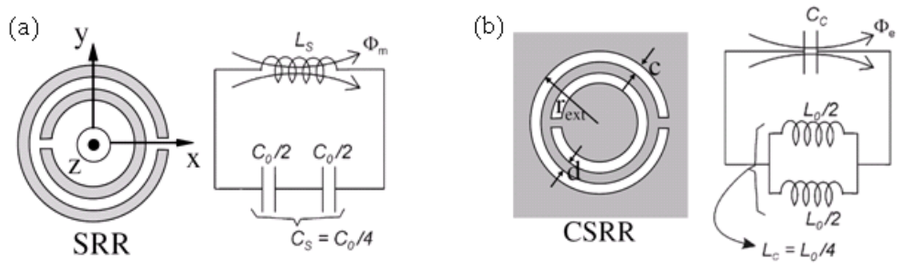


Fig. 1. Scheme of the split-ring resonator (SRR) (a) and the complementary split-ring resonator (CSRR) (b) and their equivalent circuit models. Metallic parts are depicted in grey, whereas etched parts are depicted in white.

The resonator can be modelled as is shown in Fig. 1(a) (Baena et al., 2005). $C_0/2$ is the capacitance related with each of the two SRR halves, whereas $L_s$ is the resonator self-inductance. $C_0$ can be obtained as $C_0=2\pi r C_{pul}$, where $C_{pul}$ represents the per unit length capacitance between de rings forming the resonator. As for $L_s$, it can be approximated to the inductance of a single ring with the average radius of the resonator and the width of the rings, $c$. Taking into account the circuit model of the resonator, its resonance frequency can be calculated as:

$$\omega_0 = \frac{1}{\sqrt{L_s C_s}} \tag{1}$$

As long as the inductance and the capacitance of the resonator can be increased (within the technology limits), the resonance frequency of the SRR can be decreased, reducing its electrical size.
The application of the Babinet principle to the structure of the SRR leads to its complementary counterpart: the complementary split-ring resonator (CSRR) (Falcone et al.,

2004), depicted in Fig. 2(b). In the CSRR the rings are etched on a metallic surface and its electric and magnetic properties are interchanged with respect to the SRR: the CSRR can be excited by an axial time-varying electric field and exhibits negative values of the dielectric permittivity. The equivalent circuit model of the CSRR is shown in Fig. 2(b). The resonance frequency of the CSRR is almost the same of the frequency of a SRR with the same dimensions.

Both resonators, the SRR and the CSRR can be employed in the synthesis of effective media (Smith et al., 2000; Shurig et al., 2008) and metasurfaces (Falcone et al., 2004), as well as, of course, artificial transmission lines (Martín et al. 2003; Falcone et al., 2004). Next sections will deal with the implementation of metamaterial transmission lines based on the resonant-type approach, as well as their application to microwave device design.

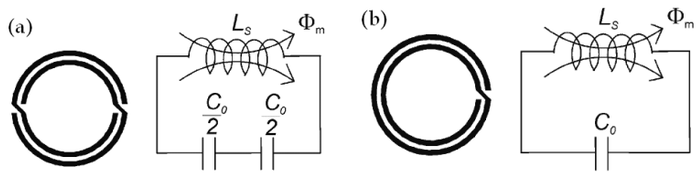


Fig. 2. SRR-based resonators and their circuit models. (a) Non-bianisotropic SRR. (b) Spiral resonator. Metallic parts are depicted in black.

Taking SRRs and CSRRs as starting points, numerous resonators have been proposed. The new resonators are obtained by modifying the topology of the original ones in order to decrease their electrical size or obtain certain symmetry properties. Figures 2, 3 and 4 show several examples of different resonators obtained following different strategies. In Fig. 2, two different resonators can be found and two more could be obtained as their complementary structures. The first one is known as non-bianisotropic split-ring resonator. It has the same electrical size as the SRR, but it has been designed to avoid the cross-polarisation (bianisotropic) effects that the original SRR exhibits (Baena et al, 2005). The electrical size can be reduced enhancing either the capacitance or the inductance of the resonator. This is achieved in the spiral resonator (Fig. 2(b)) thanks to the increase of the total capacitance of the resonator in such a way that the resonance frequency is half the one of the SRR.

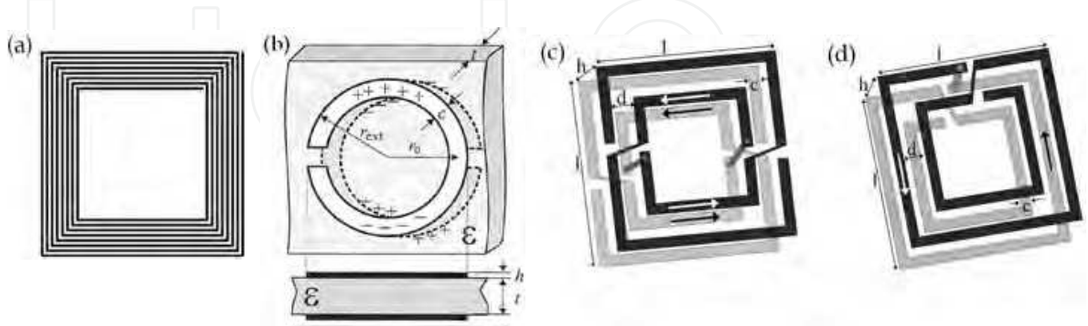


Fig. 3. SRR-based compact resonators. (a) Spiral resonator with 8 loops. (b) Broadside-coupled split-ring resonator (BC-SRR). (c) Two-layer multi spiral resonator (TL-MSR). (d) Broad-side coupled spiral resonator with four turns (BC SR (4)).

There are other strategies devoted to the miniaturisation of the resonators. One of them is the addition or enlargement of the metallic strips in order to increase the inductance of the whole structure. One example of the application of this strategy is the spiral shown in Fig. 3(a) (Alici et al., 2007; Bilotti et al., 2007). On the other hand, the capacitance can be enhanced designing the resonator so that their strips are broad-side coupled (see broad-side coupled SRR in Fig. 3(b)) (Marqués et al., 2003). This strategy requires the use of two metal layers on which lay the different parts of the resonator. By this means the strips are broad-side instead of edge-side coupled and the capacitance is enhanced, especially if thin substrates are employed. Both strategies are combined in the examples shown in Fig. 3(c) and (d) (Aznar et al., 2008b). In these two resonators the strips are elongated connecting the two metal layers by means of vias, increasing the inductance of the resonator. Additionally, the capacitance is enhanced thanks to the broadside coupling. Following these strategies, the electrical size of the resonators can be drastically reduced.

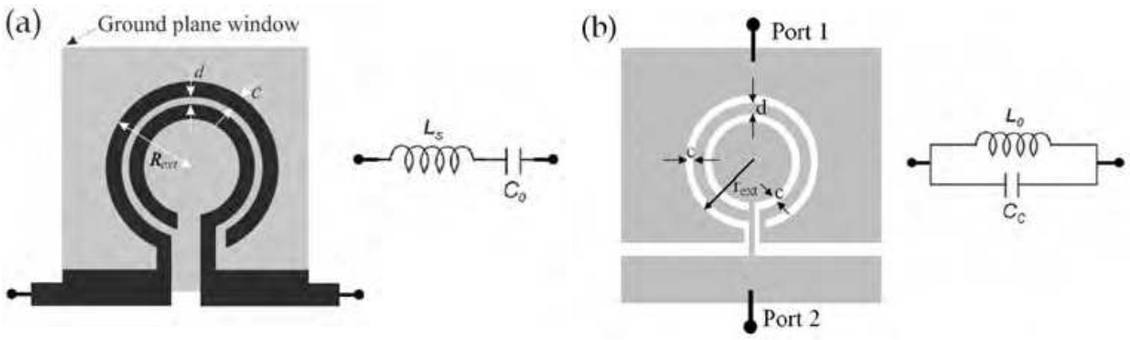


Fig. 4. (a) Open split-ring resonator (OSRR) and its equivalent circuit model. (b) Open complementary split-ring resonator (OCSRR) and its equivalent circuit model.

A different kind of SRR-based structures are open resonators. Figure 4 shows the layouts and equivalent circuit models of the open SRR (Martel et al., 2004) and the open complementary SRR (Vélez et al., 2009a). As can be seen in the layout, the OSRR is based on the SRR and is obtained by truncating the rings forming the resonator and elongating them outwards. The OCSRR can be obtained as the complementary particle of the OSRR, in a similar way as the CSRR is obtained from the SRR. The resonators shown in Fig. 4 can be implemented either in microstrip or in coplanar technology (Durán-Sindreu et al., 2009). The equivalent circuit models of the resonators are also shown in Fig. 4. The equivalent circuit model of the OSRR is a series LC resonator (Martel et al., 2004). The inductance $L_s$ can be obtained as the inductance of a ring with the average radius of the resonator and the same width, $c$, of the rings forming the OSRR. The capacitance $C_0$ is the distributed edge capacitance that appears between the two concentric rings. In a similar way, the OCSRR can be modelled by means of a parallel LC resonant tank (Vélez et al., 2009), where the inductance $L_0$ is the inductance of the metallic strip between the slot hooks and the capacitance is that of a disk with radius $r_0$-$c$/2 surrounded by a metallic plane separated by a distance $c$.

The small size of all these resonant particles makes them suitable for the implementation of microwave devices based on resonant-type metamaterial transmission lines with small dimensions and even new functionalities. This will be illustrated in the following sections.

## 3 Resonant-type Metamaterial Transmission Lines

The previously presented resonators can be employed in many different applications and, as has already been pointed out, one of them is the implementation of metamaterial transmission lines. Soon after the implementation of the first negative refraction index medium (Smith et al., 2000), the same concepts were applied to the synthesis of planar one dimensional media, giving rise to the first left-handed transmission lines (Eleftheriades et al., 2002; Caloz & Itoh, 2002). This first approach devoted to the implementation of metamaterial transmission lines consisted on periodically loading a conventional transmission line with series capacitive and shunt-connected inductive elements. Some examples of such lines can be found in Fig. 5 together with the equivalent circuit model of the unit cell. The loading elements are modelled by $C_L$ and $L_L$, whereas $L_R$ and $C_R$ represent the line elements.

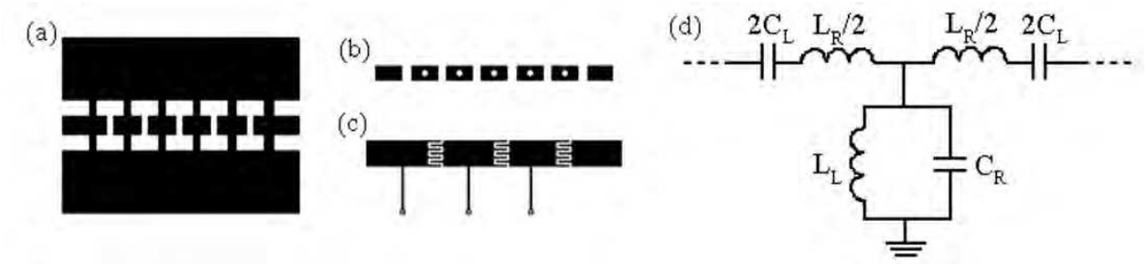


Fig. 5. Examples of CRLH transmission lines based on the LC-loaded transmission line approach and their equivalent circuit model. (a) Conventional coplanar waveguide transmission line loaded with capacitive gaps and metallic connections to the ground planes. (b) Conventional microstrip transmission line loaded with capacitive gaps and vias. (c) Conventional microstrip transmission line loaded with interdigital capacitors and shunt connected inductive stubs. (d) Equivalent circuit model for the LC-loaded transmission line unit cell.

In such a medium, we can express the dispersion relation of such lines as:

$$\cos(\phi) = 1 + \frac{Z_s(\omega)}{Z_p(\omega)} \tag{2}$$

where $Z_s$ and $Z_p$ are the series and shunt impedance of the circuit model, respectively. This expression gives rise to the generic dispersion diagram shown in Fig. 6 (a) (regions corresponding with positive group velocity have been chosen). Two transmission bands can be identified: the first one corresponds to the left-handed propagation region, in which the propagation constant is negative, whereas in the second one the propagation is right-handed. Moreover, the effective dielectric permittivity and magnetic permeability can be obtained from the values of the series impedance and the shunt admittance, respectively, revealing the frequency dependence of the sign of $\varepsilon_{eff}$ and $\mu_{eff}$ that gives rise to the different right and left-handed bands (Marqués et al., 2008). At those frequencies in which the propagation is dominated by the loading elements, the propagation is left-handed ($\beta$<0 region), whereas the parasitic line elements give rise to the right-handed transmission band ($\beta$>0 region). This composite behaviour gives the name composite right/left-handed (CRLH) to these transmission lines. Both transmission bands are usually separated by an intermediate frequency gap in which transmission is forbidden (See Fig. 6(a)). However, it is

possible to force both limits of the gap ($\omega_{G1}$ and $\omega_{G2}$) to coincide ($\omega_{G1}=\omega_{G2}=\omega_0$) in order to make it disappear (Caloz & Itoh, 2005). In this case, known as balanced case, a continuous transition between the left- and the right-handed transmission bands is obtained giving rise to a wide band exhibiting backward and forward propagation at different frequencies (Fig. 6(b)).

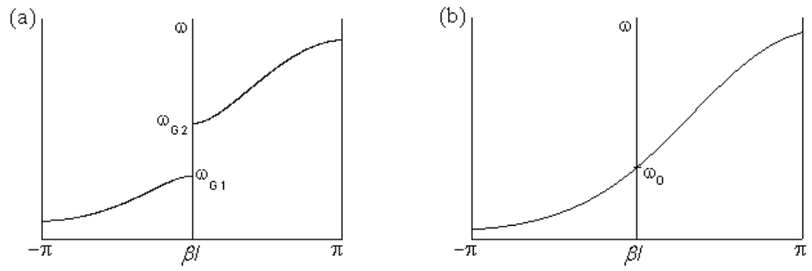


Fig. 6. Dispersion diagrams of a CRLH transmission line (a) for the unbalanced case (b) for the balanced case.

A second approach devoted to the implementation of composite right/left-handed transmission lines was proposed by some of the authors soon after the works presenting the LC-loaded transmission line: the resonant-type approach (Martín et al., 2003). In this approach, subwavelength resonators like the ones presented in the previous section are used to (in combination with other elements) load conventional transmission lines and obtain CRLH artificial lines.

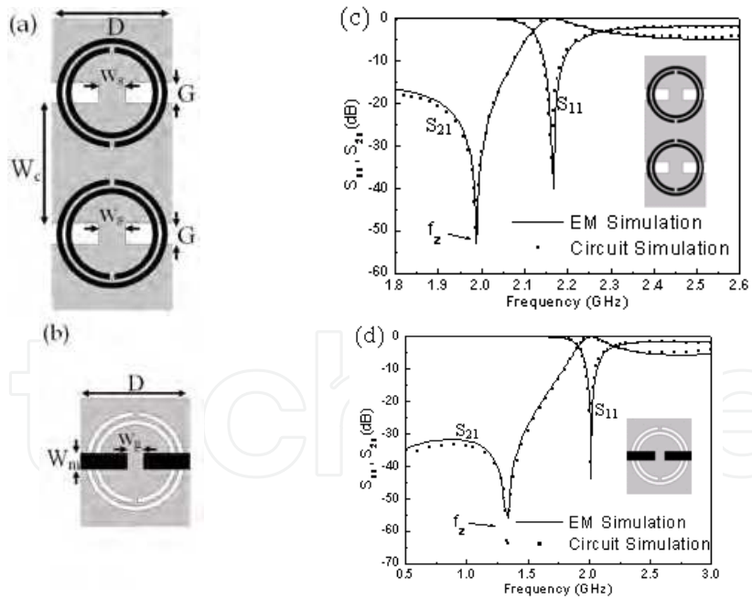


Fig. 7. Layouts and frequency responses of two resonant-type metamaterial transmission line unit cells. Metallic parts are depicted in black for the top and in gray for the bottom layer of the substrate. (a) SRR-based CRLH transmission line implemented in coplanar technology. (b) CSRR-based CRLH transmission line implemented in microstrip technology. (c) Frequency response of the structure shown in (a). (d) Frequency response of the structure shown in (b).

This approach allows the use of both, metallic and complementary resonators in coplanar and microstrip technology (see Fig. 7). Thanks to the small size of the loading resonators, the resulting transmission lines are compact and can be employed in the design of microwave devices with reduced dimensions employing commercial substrates. The location of SRRs on the bottom layer of a coplanar waveguide allows the excitation of the resonators by the magnetic field and provides negative values of the magnetic permeability. In order to obtain left-handed propagation, negative dielectric permittivity is also required, what is obtained by means of metallic junctions between the line and the ground planes (see Fig. 7 (a)) (Martín et al., 2003). It is also possible to use SRRs to load a microstrip transmission line locating them on the top layer of the substrate, close to the signal strip. By this means, the SRRs are excited by the magnetic field and, if they are combined with vias, provide a left-handed transmission band in a certain frequency range in the vicinity of the resonance frequency of the rings. Of course, the effect of the parasitic line elements provides a second transmission band with right-handed characteristics; in other words: resonant-type metamaterial transmission lines do also exhibit a composite behaviour. This allows the design of balanced transmission lines, which are interesting for broadband applications (Gil et al., 2007a).

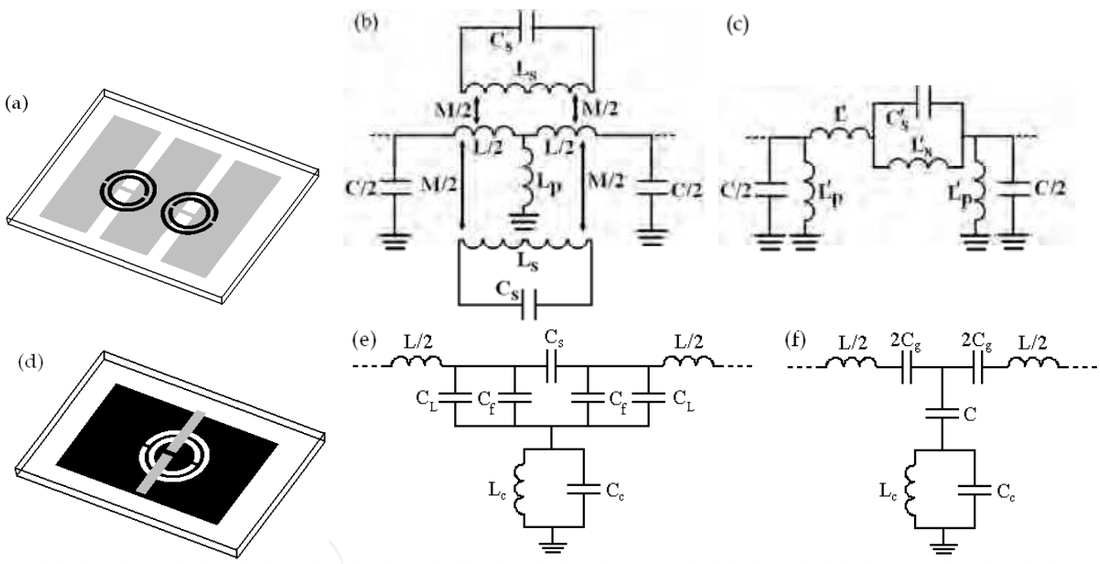


Fig. 8. Schemes of two resonant-type metamaterial transmission lines and their equivalent circuit models. Metallic parts are depicted in black for the bottom and in gray for the top layer of the substrate. (a) SRR-based transmission unit cell. (b) Equivalent circuit model for the structure shown in (a). (c) Modified circuit model for the structure shown in (a). (d) CSRR-based unit cell. (e) Equivalent circuit model for the structure shown in (d). (f) Modified circuit model for the structure shown in (d).

Other resonators can be employed as well in the design of this kind of metamaterial transmission lines, as is the case of CSRRs. In this case, the most usual configuration is the one in which the resonators are etched on the ground plane of a microstrip transmission line and combined with capacitive gaps etched on the signal strip (see Fig. 7(b)) (Falcone et al., 2004), although other configurations are possible (Gil et al., 2008a). The response of both

structures (SRR- and CSRR-based) (performed with the *ADS Momentum* commercial simulation software), which are very similar, can be observed in Fig. 7. They both exhibit a left-handed transmission band preceded by a transmission zero, which represents the main difference with respect to the LC-loaded transmission line approach given that in that case the transmission zero is found at the origin. The right-handed band appearing above the left-handed one is not shown in the graphs. In Fig. 7 the electromagnetic simulations of the structures are compared with the responses given by their equivalent circuit models, which can be found in Fig. 8. As can be seen, the models perfectly describe the behaviour of the structures at the frequency range of interest.

For the SRR-based unit cell (Fig. 8(a)) the circuit model is the one shown in Fig. 8 (b). The resonators are modelled by the resonant tanks formed by $L_s$ and $C_s$, which are coupled to the line by means of the mutual inductance $M$. The line parameters are $L$ and $C$, whereas $L_p$ represents the metallic strips. This model is the improvement of a previously existing one (Martín et al, 2003) and the parameters have a more realistic physical meaning and provide a better description of the behaviour of the structure (Aznar et al., 2008a). Nevertheless, both, the former and the new proposed model can be transformed into the circuit shown in Fig. 8(c) which, as is shown in Fig. 7, reproduces the response of the structure in a very proper way. The transformation equations are the following ones:

$$L_s' = 2M^2 C_s \omega_o^2 \frac{\left(1+\frac{L}{4L_p}\right)^2}{1+\frac{M^2}{2L_pL_s}} \tag{3}$$

$$C_s' = \frac{L_s}{2M^2\omega_o^2}\left(\frac{1+\frac{M^2}{2L_pL_s}}{1+\frac{L}{4L_p}}\right)^2 \tag{4}$$

$$L' = \left(2+\frac{L}{2L_p}\right)\frac{L}{2} - L_s' \tag{5}$$

$$L_p' = 2L_p + \frac{L}{2} \tag{6}$$

and they allow the calculation of the parameters of the circuit (c) in terms of the parameters of the circuit (b). The inversion of these equations provides the opposite transformation. Circuit (c), much simpler, is usually the one used to study the behaviour of the structure and perform parameter extractions.

Regarding the CSRR-based structure (Fig. 8(d)), a new and improved circuit model has also been recently proposed. It is the circuit shown in Fig. 8(e), which provides a more accurate description of the behaviour of the structure and is able to explain certain discrepancies that the previous one, which is shown in Fig. 8(f), presented. In the circuit (e), the resonator is modelled by the resonant tank formed by $L_c$ and $C_c$ , the line parameters are $L$ and $C_L$ and the gap is modelled by the π-structure formed by $C_s$ and $C_f$, which take into account the

series and the fringing capacitances due to the presence of the capacitive gap. The circuit (f) is perfectly able to reproduce the behaviour of the structure, as can be corroborated in Fig. 7(b), where its response is compared with the electromagnetic simulation of the structure. Nevertheless, circuit (e) can be transformed into circuit (f), by means of the following equations:

$$C_{par} = C_f + C_L \tag{7}$$

$$2C_g = 2C_s + C_{par} \tag{8}$$

$$C = \frac{C_{par}(2C_s + C_{par})}{C_s} \tag{9}$$

so that the circuit (f), much simpler can substitute circuit (e) for a more straightforward work. Circuit (f), in which $C$ was formerly interpreted merely as the coupling capacitance between the line and the resonator and $C_g$ was the gap capacitance, didn't predict neither the important change that $C$ experiences nor the change on the position of the transmission zero (given by expression (10)) that occurs when the capacitive gap is eliminated. However, expressions (7) to (9) predict perfectly this behaviour (Aznar et al, 2008c).

$$\omega_z = \frac{1}{\sqrt{L_c(C + C_c)}} \tag{10}$$

As has already been pointed out, circuits shown in Fig. 8(c) and (f) are able to reproduce the response of the structures (a) and (d). This is illustrated in Fig. 7, where the full wave simulations of both structures are compared with the responses of their equivalent circuit models. The values of the circuit elements employed to obtain the compared responses have been obtained applying a parameter extraction method suitable for each of the structures. The parameter extraction method consists on the imposition of several conditions obtained either from a simulated or a measured response of one of the structures in order to obtain the necessary conditions to obtain the values of all the parameters of the circuit. In both structures, the model is formed by five circuit elements, so the number of impositions must also be five. The first of the parameter extraction methods was the corresponding to the CSRR-based structure (Bonache et al., 2006b), whereas the method for the SRR-based structure was proposed later (Aznar et al., 2008d). The main differences between both methods are due to the fact that they are based on a T- and a π-model, respectively. In both methods, two structures are employed: the first one contains all elements and, in the second one, the capacitive gap (or the metallic strips in the case of the SRR-based unit cell) is eliminated (see Fig. 9). This allows the determination of the five circuit elements in both cases. In the example shown in Fig. 9 the extraction is carried out from the measurement of the fabricated structure and losses have been taken into account by means of $R$. Its value has been adjusted by tuning until matching of the insertion loss level is achieved.

In the first of the methods, corresponding with the CSRR-based structure modelled by a T-circuit model, the imposed conditions are the transmission zero frequency (given by expression (13)), the frequency at which the phase is 90º and the resonance frequency of the resonator. The two first frequencies can be directly identified from the representation of the

$S_{21}$ parameter (from the magnitude and the phase), whereas the third one can be identified from the representation of the $S_{11}$ parameter in the Smith Chart (see Fig.10).

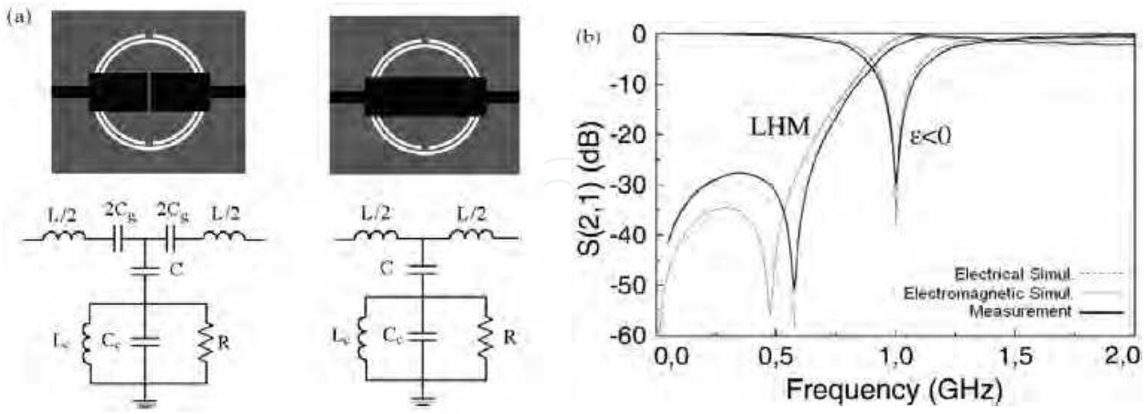


Fig. 9. (a) Layouts and circuit models of the structures employed in the parameter extraction method for the CSRR-based unit cell. (b) Frequency responses of the measurement, the electromagnetic simulation and the electric simulation employing the extracted parameters.

The resonance frequency of the CSRR has a particularity: at that frequency, the parallel branch opens and the input impedance is formed just by the impedance of the output port and the series branch impedance. This means that the real part of this impedance is the output port impedance (usually 50 ohm) and the imaginary part is given by the series branch impedance which consists of an inductance in the case of the structure without gap and an inductance and a capacitance in the case with gap.

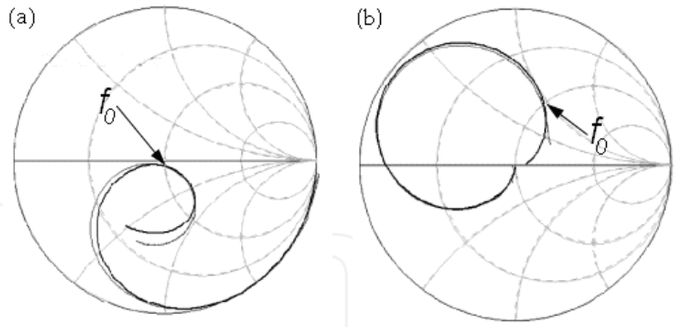


Fig. 10. Representation of the $S_{11}$ parameter for the identification of the CSRR resonance frequency (a) for the complete (LH) structure (b) for the structure without gap (ε<0). Measurement and electric simulation.

The resonance frequency can be found at the point where the $S_{11}$ curve meets the unit resistance circle in the Smith Chart. Given that the reactance of the input impedance at this point can be read from the chart, the calculation of the series branch elements can be easily carried out from the curves of both structures. In the case of the complete structure, at the resonance frequency the series branch is capacitive, whereas in the structure without gap it is inductive (see Fig. 10). By this means, we obtain three of the five necessary conditions, that is, the resonance frequency of the rings, which is $\omega_0 = 1/(L_c C_c)^{1/2}$, and the values of the

reactance for both structures, which allow us to obtain the values $L$ and $C_g$. As has been previously mentioned, the two other necessary conditions will be the transmission zero frequency and the 90º-phase frequency, at which the series and shunt impedances of the circuit have opposite signs ($Z_s$=-$Z_p$) (Bonache et al., 2006b). Once the parameters have been extracted, the electric simulation presents a very good fitting with the original curve (simulation or measurement), as figures 7, 9 and 10 corroborate.

In the case of the SRR-based structures, the parameter extraction method is very similar, but with the corresponding modifications for a π-circuit. As in the previous case, two different structures can be employed: a complete structure and a second one without metallic strips connecting the line with the ground planes. The 90º-phase and the transmission zero frequencies are imposed as well. However, the expression for the transmission zero frequency is in this case the following:

$$\omega_z = \frac{1}{\sqrt{L'_s C'_s}} \tag{11}$$

which is the frequency at which the series branch opens. One more useful frequency is that at which the series impedance nulls. When that happens, the input impedance is formed just by the impedance of the output port and the shunt impedance. This will correspond with the point in the Smith Chart in which the $S_{11}$ curve crosses the unit conductance circle and the subsceptance of the input impedance can be directly read from the Smith Chart. This subsceptance corresponds with the shunt admitance of the structure, which is formed by an inductance and a capacitance in the case of the complete structure and only a capacitance in the structure without metallic strips. This allows the determination of the frequency at which the series impedance nulls, $w_s$, which can be obtained as:

$$\omega_s = \sqrt{\frac{1}{L'_s C'_s} + \frac{1}{L' C'_s}} \tag{12}$$

as well as the determination of the elements of the shunt impedance, $L'_p$ and $C$. As occurred in the previous one, this parameter extraction method provides a very good fitting between the electrical response given by the extracted parameters and the original curve.

Similar parameter extraction methods have been recently applied to structures based on open split-ring resonators (OSRRs) and open complementary split-ring resonators (OCSRRs) (Fig. 11 (a) and (d), respectively). The followed strategy is very similar to the previous ones and it is even simpler, given that the equivalent circuit models consist in just three elements (see Fig. 11 (c) and (f)). In order to provide a good description of the structure, in both cases a small but not negligible phase shift must be taken into account at both sides of the resonator ( Fig. 11 (b) and (e)). Taking this into account, the resulting equivalent circuit models are the ones shown in Fig. 11 (c) and (f). For the parameter extraction of the OSRR circuit, the imposed conditions are the following ones. As in the previous case, the frequency at which the series impedance nulls is found in the Smith Chart as the point in which the curve crosses the unit conductance circle, what occurs at:

$$\omega_{Zs=0} = \frac{1}{\sqrt{L'_s C_s}} \tag{13}$$

This gives us also the value of the shunt capacitance, which can be obtained from the value of the susceptance of the input impedance at that frequency. In addition, the reflection zero frequency, at which the characteristic impedance of the structure is matched to the ports (usually 50 Ω), is also identified and imposed, being the expression of the characteristic impedance:

$$Z_O = \sqrt{\frac{Z_s(\omega)Z_p(\omega)}{2Z_s(\omega)+Z_p(\omega)}} \tag{14}$$

and from it, the third of the parameters of the circuit can be obtained. The method employed for open complementary split-ring resonators is very similar. One of the imposed frequencies is the one at which the shunt impedance opens:

$$\omega_{Zp\to\infty} = \frac{1}{\sqrt{L'_p C'_p}} \tag{15}$$

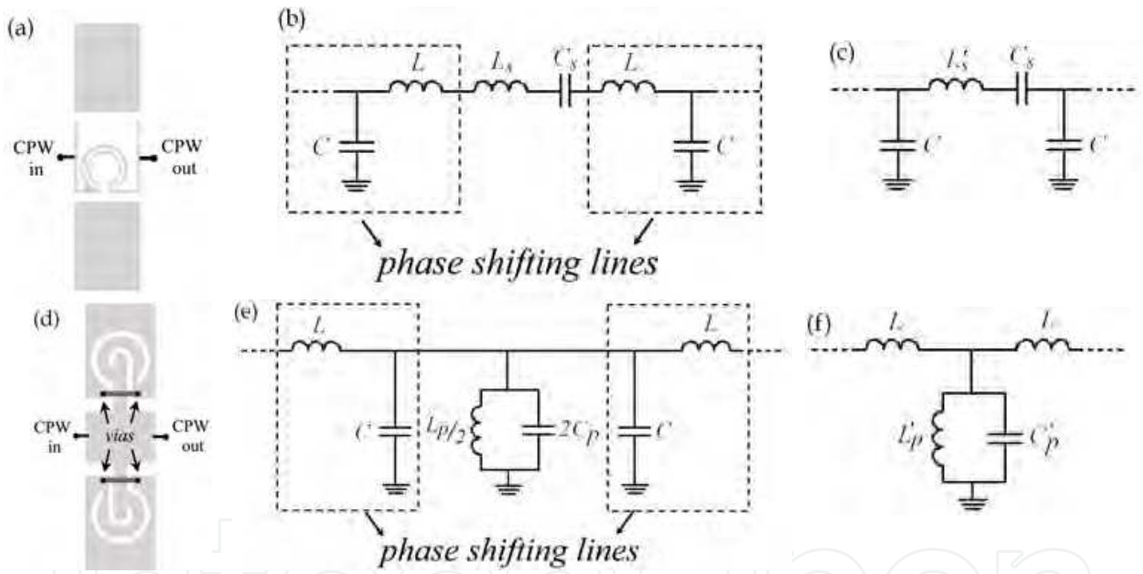


Fig. 11. (a) Layout of an OSRR implemented in coplanar waveguide technology. (b) Equivalent circuit model taking into account the phase shifting lines. (c) Simplified equivalent circuit model. (d) Layout of an OCSRR implemented in coplanar waveguide technology. (e) Equivalent circuit model taking into account the phase shifting lines. (f) Simplified equivalent circuit model.

This frequency can be found as the point where the $S_{11}$ curve crosses the unit resistance circle in the Smith Chart and the value of the corresponding reactance of the input impedance gives us also the value of the series inductance, *L*. Furthermore, the characteristic impedance of the structure is forced to be matched to the ports at the reflection zero frequency, giving rise to the following expression:

$$Z_O = \sqrt{Z_s(\omega)(Z_s(\omega) + 2Z_p(\omega))} \tag{16}$$

With these three conditions, all parameters of the equivalent circuit model can be determined. For both structures, the frequency response of the circuit model properly fits the electromagnetic simulation of the structure (see Fig. 12).

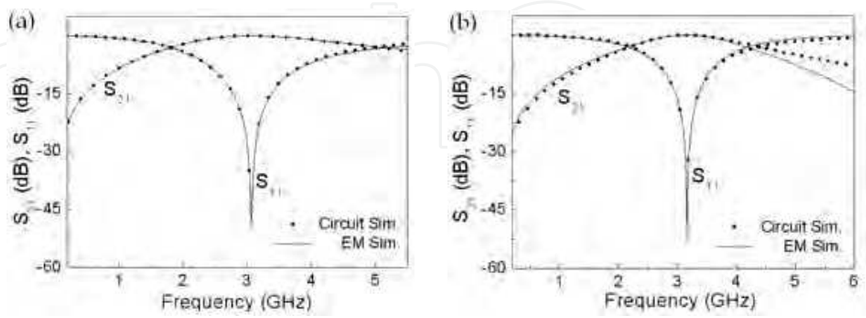


Fig. 12. Electromagnetic and electric simulations of the structures shown in Fig.11 (a) and (d). The electric parameters have been obtained by means of the described parameter extraction method. (a) Simulations of the OSRR structure. (b) Simulations of the OCSRR structure.

OSRR and OCSRR structures can be cascaded to implement composite right/left-handed transmission lines with controllable characteristics for their use in the design of microwave devices (Durán-Sindreu et al., 2009).
These results prove the validity of the proposed circuit models, as well as the diverse developed parameter extraction methods, which are an important tool in the design of this kind of artificial transmission lines.

## 4. Applications

Metamaterial transmission lines have two main characteristics which make them very interesting for the design of microwave devices. One of them is their small size, which allows device miniaturisation. The second one is the controllability of their electrical characteristics, that is, the characteristic (or Bloch) impedance $Z_0$ and the electrical length, $\beta l$. Such controllability is higher than in conventional transmission lines, where these magnitudes strongly depend on the line dimensions, determining the size of the final device requiring specific values of the line characteristics. Artificial transmission lines, however, offer the possibility of tailoring these properties to some extent (Gil et al., 2006), allowing the design of very competitive devices, even with new functionalities.
Simple examples of microwave devices including transmission lines with specific values are power dividers. They can be implemented by means of resonant-type metamaterial transmission lines and an important size reduction can be achieved (Gil et al., 2007b, Aznar et al., 2009b). Figure 13 shows one example of power dividers implemented by means of metamaterial impedance inverters, in which the impedance and the electrical length have been tailored to exhibit the required values at the design frequency ($f_0$=1.5 GHz). Figure 13(a) compares the layouts of two power dividers implemented in microstrip technology. The first one employs two resonant-type metamaterial transmission lines based on CSRRs as

impedance inverters with $Z_0$=70.71Ω and $\beta l$=90º. In the second one, the inverters are conventional transmission lines.

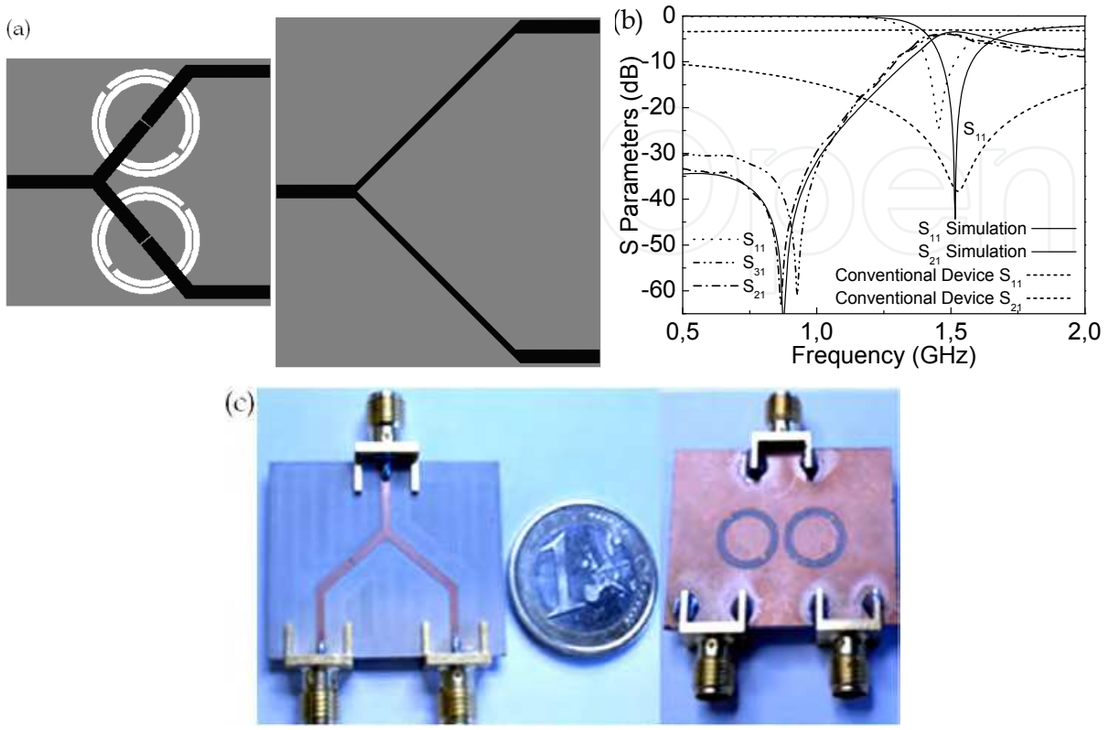


Fig. 13. (a) Comparison between the layouts of a conventional and a "metadivider" formed by two impedance inverters. (b) Frequency response of the power dividers shown in (a). (c) Photograph of the fabricated device. The device has been implemented employing a commercial substrate with thickness $h$=1.27mm and $\varepsilon_r$=10.2. The dimensions of the metamaterial inverters are: inverter length $l$=12.5mm, gap width $g$=0.16mm, CSRR external radius $r_{ext}$= 4.76mm, ring with $c$=0.5mm.

The metamaterial inverters have approximately half the length of the conventional ones so, thanks to their use, a 50% of size reduction can be achieved. Taking into account the frequency response of both devices (Fig. 13(b)), it can be seen that they exhibit similar loss levels (close to the ideal value, -3dB) at the design frequency, although the bandwidth of the metamaterial divider is narrower. This kind of dividers is, therefore, suitable for narrow band applications in which the size reduction is an important aspect. Other resonators and kinds of metamaterial transmission lines can be employed to implement similar power dividers (Aznar et al., 2009b, Gil et al., 2008b).

This kind of transmission lines can also be applied for bandwidth enhancement purposes (Sisó et al., 2007). Figure 14 shows a rat-race hybrid employing four metamaterial inverters. Three of them are right-handed inverters ($\beta l$=+90º), whereas a left-handed inverter with $\beta l$=-90º substitutes for the 270º inverter present in conventional hybrids.

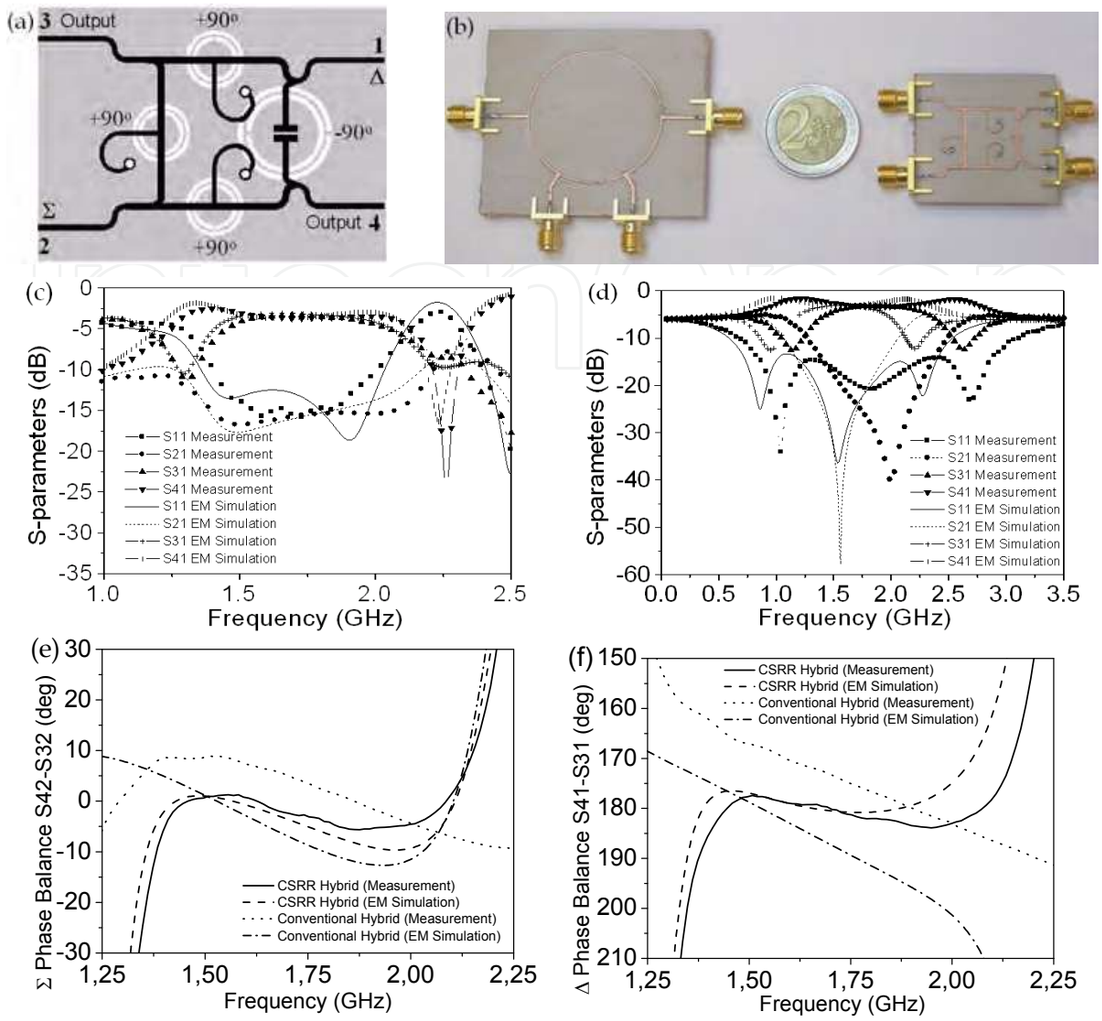


Fig. 14. (a) Layout of a rat-race hybrid coupler implemented by means of metamaterial transmission lines. The device has been implemented employing a commercial substrate with thickness $h$=635μm and $\varepsilon_r$=10.2. The relevant dimensions of the metamaterial inverters are, for the +90º inverters: stub length $l$=11.50mm, CSRR external radius $r_{ext}$=3.14mm, ring width $c$=0.34mm; for the -90º inverter $l$=10.2mm, gap separation $g$=0.37mm, gap width $w$=2.57, external resonator radius $r_{ext}$=5.1mm, ring width $c$=0.44mm. (b) Comparison between the sizes of a conventional and a metamaterial coupler. (c) S-parameters for the metamaterial coupler. (b) S-parameters for the conventional coupler. (e) Comparison of the phase balance of the Σ-port for the conventional and the metamaterial coupler. (f) Comparison of the phase balance of the Δ-port for the conventional and the metamaterial coupler.

As a result, the total size of the device is about 3 times smaller than a conventional one (see comparison in Fig. 14 (b)). Power splitting, isolation and matching of the metamaterial hybrid are similar to the ones of a conventional one (Fig. 14 (c) and (d)). Nevertheless, as can be seen in Fig. 14 (e) and (f), the phase balance presents a broader bandwidth than a

conventional device. The dispersion diagram has been controlled to make the phase difference between the corresponding lines keep almost constant over a wider range. By these means, not only the size is minimized, but also the bandwidth of the device is improved.

As has been previously mentioned, the controllability of the line characteristics of metamaterial transmission lines opens the door to new application and functionalities (Sisó et al., 2009). Nowadays, there is an increasing interest in devices exhibiting multi-band operation. However, conventional transmission lines do not offer the possibility of designing such components working at arbitrary chosen frequencies. The manipulation of the dispersion diagram of metamaterial transmission lines allows the design of multi-band devices in which the operation frequencies can be chosen within certain margins. This can be achieved thanks to the composite behaviour of such transmission lines, given that the different operation frequencies can be chosen at the different transmission bands that these lines exhibit (Bonache et al., 2008; Sisó et al., 2008b).

If we consider the CSRR-based transmission line (Fig. 8(d)) and its equivalent circuit model (Fig. 8(f)), we can express the dispersion relation and the characteristic impedance of the structure as:

$$\cos(\phi) = 1 + \frac{Z_s(\omega)}{Z_p(\omega)} \tag{17}$$

$$Z_0 = \sqrt{Z_s(\omega)(Z_s(\omega) + 2Z_p(\omega))} \tag{18}$$

Impedance inverters are widely employed in microwave devices, so we will consider the design of a dual-band impedance inverter. It involves the imposition of the required phase ($\phi_1$=-90º, $\phi_2$=+90º) and impedance ($Z_1$, $Z_2$) values at the two frequencies of interest ($f_1$, $f_2$). The elements of the circuit model can be expressed in terms of these values. Given that the imposition of the phase and impedance represent four conditions, one more condition must be imposed in order to univocally determine the five parameters of the circuit model (Fig. 8(f)). This additional imposition can be, for example, the balance condition. In this case, the circuit elements can be expressed as:

$$L = \frac{2(Z_1\omega_1 + Z_2\omega_2)}{\omega_2^2 - \omega_1^2} \tag{19}$$

$$C_g = \frac{\omega_2^2 - \omega_1^2}{2\omega_1\omega_2(Z_1\omega_2 + Z_2\omega_1)} \tag{20}$$

$$C = \frac{2(Z_1\omega_2 + Z_2\omega_1)}{(Z_2^2 - Z_1^2)\omega_1\omega_2} \tag{21}$$

$$C_c = \frac{Z_1\omega_2 + Z_2\omega_1}{(\omega_2^2 - \omega_1^2)Z_1Z_2} \tag{22}$$

$$C_g = \frac{(Z_1\omega_1 + Z_2\omega_2)(\omega_2^2 - \omega_1^2)Z_1Z_2}{\omega_1\omega_2(Z_1\omega_2 + Z_2\omega_1)^2} \tag{23}$$

It can be observed that all parameters, except $C$, are positive as long as $\omega_2>\omega_1$. The capacitance $C$, however, can be negative if $Z_2<Z_1$, or even infinity if $Z_2=Z_1$ (as most applications require). From this, it can be concluded that, employing the considered structure, the synthesis of impedance inverters with the same impedance value at two operating frequencies requires the use of non-balanced structures (Bonache et al., 2008).
An application example a of dual-band impedance inverter designed by means of CSRRs can be seen in Fig. 15 (Sisó et al., 2008a). The device has been designed to work at the mobile GSM bands ($f_1$=0.9GHz and $f_2$=1.8GHz). At these frequencies, the CSRR-based impedance inverter exhibits the required values of impedance ($Z_0$=35.35Ω) and phase ($\beta l_1$=-90º at $f_1$ and $\beta l_2$=+90º at $f_2$). Figure 15 (b) shows these two magnitudes, whereas Fig. 15 (c) shows the performance of the whole power divider. It can be seen that both, the inverter and the divider behave as expected at the design frequencies. The use of a metamaterial transmission line as impedance inverter allows the reduction of the final device size as well as the dual-band operation. The design of devices working at more than two bands is under study. Several generalized models for multiband operation have been proposed (Eleftheriades, 2007; Sisó et al., 2008c) and implementations by means of the CL-loaded approach have been already carried out (Papanastasiou et al., 2008).

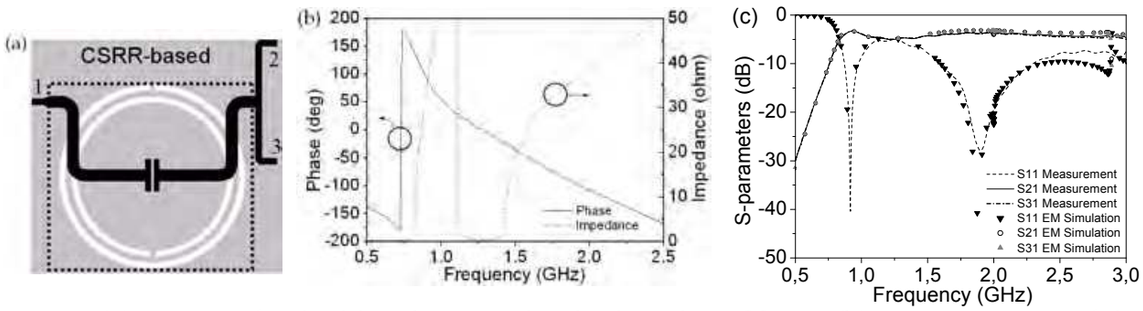


Fig. 15. (a) Layout of a dual-band power divider based on CSRRs. (b) Representation of the phase and the impedance of the inverter used in the implementation of the power divider shown in (a). (c) Simulated and measured frequency response of the power divider. The device has been implemented employing a commercial substrate with thickness $h$=635μm and $\varepsilon_r$=10.2. The metamaterial inverter dimensions are: marked active area $A$= 17.7mm x 15.8mm, resonator external radius $r_{ext}$=7.9mm, ring width $c$=0.5mm, line width $w$=1.0mm, gap separation $g$=0.27mm.

The fact that resonant-type metamaterial transmission lines exhibit a frequency selective behaviour suggests their application in filter design. This group has developed during the last years a wide work in this field, designing several kinds of filters based on subwavelength resonators (Gil et al., 2008b). The different responses that these structures provide allow the design of several kinds of filters, like low pass, high pass and band pass filters. Broadband filters, for example, can be designed making use of balanced transmission lines, whereas non balanced lines can be used for narrow band pass filter design. Hybrid structures, for example, can be used for both, narrow and broadband filters. The hybrid approach is based on the structure combining complementary resonators and capacitive gaps and includes shunt connected inductive stubs (see Fig.16a), which contribute to obtain inductive shunt impedance and provide more design flexibility. The addition of the stubs also creates an additional transmission zero above the left handed transmission band, which

can be used in the design of filters with important frequency selectivity and very symmetric responses.

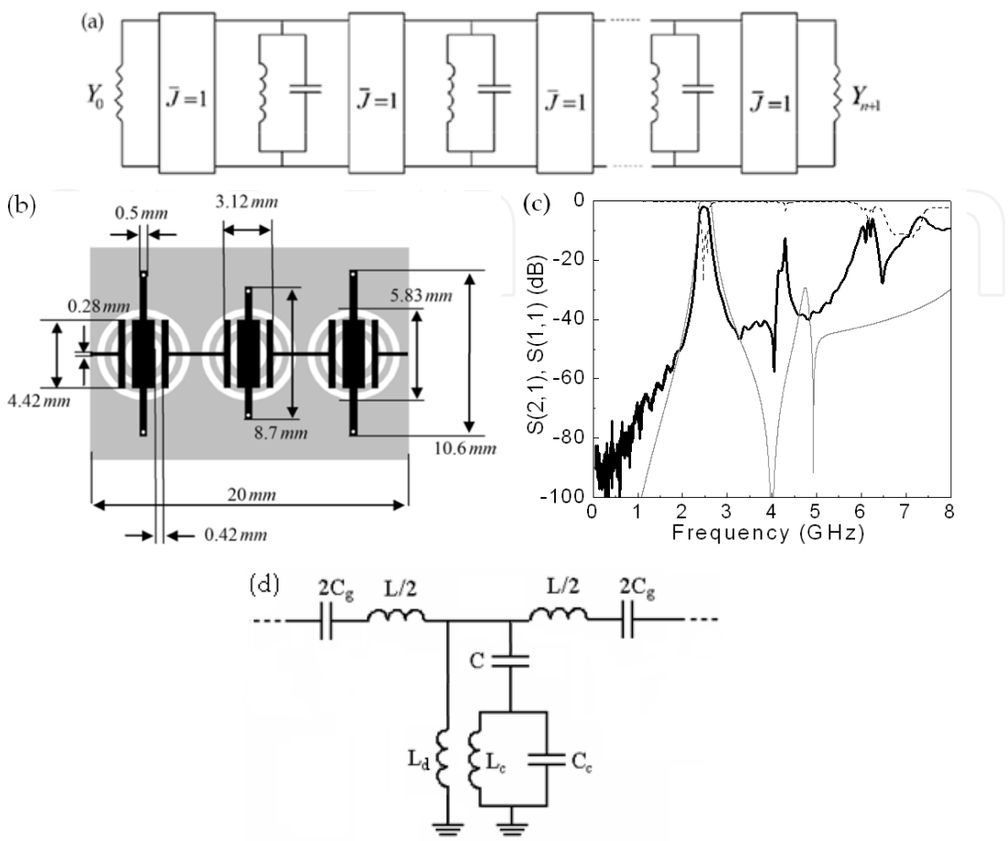


Fig. 16. (a) Band pass filter network with impedance inverters and LC resonant tanks as shunt resonators (b) Layout of a Chebyshev filter based on a hybrid structure and relevant dimensions. The device has been implemented employing a commercial substrate with thickness $h$=1.27mm and $\varepsilon_r$=10.2. (c) Electrically simulated and measured frequency response of the filter shown in (b). (d) Electrical circuit model of the hybrid unit cell.

The hybrid structure allows, for example, the design of band pass filters under standard (Chebyshev, for example) approximations with controllable bandwidth and compact dimensions (Bonache et al., 2006a). The design flexibility of these structures allows to control the position of the transmission zeros, the filter bandwidth, the ripple, etc so that a complete design methodology can be applied. The model shown in Fig. 16(a) can be applied to this structure as a basis for standard moderate and narrow band-pass filter design. When designing Chebyshev filters, the element values of the low pass filter prototype, $g_i$ can be determined by the order and ripple level. Additionally, the bandwidth of each resonator ($\Delta_i$) is set by the filter fractional bandwidth. These parameters, together with the filter central frequency and the position of the transmission zero allow the determination of all necessary circuit parameters. Each of the unit cells forming the filter is designed to, on the whole, exhibit characteristic impedance equal to the reference impedance of the ports ($Z_0$=50Ω) and phase $\phi$=90º at the considered central frequency of the pass band. By this means, one unique unit cell acts as a resonator and exhibits the required phase without needing the addition of

different stages acting as inverters and resonators, what involves a considerable size reduction. Furthermore, the series and shunt impedances have to be set to $Z_s$=-$jZ_0$ and $Z_p$=$jZ_0$, respectively, at $f_0$. The 3dB bandwidth:

$$\Delta = \frac{\omega_2 - \omega_1}{\omega_0} \tag{24}$$

and the transmission zero position:

$$f_z = \frac{1}{2\pi\sqrt{L_c(C_c + C)}} \tag{25}$$

are also imposed to determine all required elements. The bandwidth for a parallel resonant tank can be expressed in terms of its capacitance $C_{eq}$ and inductance $L_{eq}$ as:

$$\Delta = \frac{2}{Z_0}\sqrt{\frac{L_{eq}}{C_{eq}}} \tag{26}$$

These parameters can be related with the low pass prototype element values by the expressions

$$C_{eq} = \left[\frac{1}{FBW\omega_0 Z_0}\right] g_i \tag{27}$$

and

$$L_{eq} = \frac{1}{\omega_0^2 C_{eq}} \tag{28}$$

what allows us to obtain the following expression for the resonator bandwidth:

$$\Delta_i = \frac{2FBW}{g_i} \tag{29}$$

The two 3dB frequencies can be chosen to be equidistant to the central frequency, $f_0$. Considering that the series impedance is roughly constant within the pass band, the two 3dB frequencies can be considered to be those at which the shunt impedance is $Z_0/2$ and infinity, respectively, whereas it is $Z_0$ at $f_0$. These conditions can be expressed as:

$$\frac{L_d L_c \omega_1^3 (C + C_c) - L_d \omega_1}{L_c \omega_1^2 (C + C_c) - C\omega_1^2 L_d (L_c C_c \omega_1^2 - 1) - 1} = \frac{Z_o}{2} \tag{30}$$

$$L_c\omega_2^{\,2}(C+C_c)-C\omega_2^{\,2}L_d(L_cC_c\omega_2^{\,2}-1)-1=0 \tag{31}$$

$$\frac{L_dL_c\omega_o^{\,3}(C+C_c)-L_d\omega_o}{L_c\omega_o^{\,2}(C+C_c)-C\omega_o^{\,2}L_d(L_cC_c\omega_o^{\,2}-1)-1}=Z_o \tag{32}$$

what, together with expression (25) leads us to the values of the shunt impedance elements. Finally, if the series inductance is neglected, the series capacitance can be expressed as:

$$C_g=\frac{1}{2Z_o\omega_o} \tag{33}$$

This methodology has given rise to very competitive filters. Figure 16 shows the layout and frequency response of an order-3 band pass filter designed following this strategy. As can be seen, very symmetric and selective responses can be obtained and the resulting devices are very compact. The layout of the device shown in Fig. 16a has a length of 0.4λ, λ being the signal wavelength at the central filter frequency.

Purely resonant and hybrid structures can be balanced to implement broadband filters (Selga et al., 2009; Gil et al., 2007c; Gil et al., 2007d). With such lines, broad responses are obtained as a result of forcing the frequency band gap that usually separates the left- and the right-handed transmission bands to disappear. As Fig. 17 shows, high pass and band pass filters can be implemented by means of balanced transmission lines. Purely resonant structures (Fig. 17(a)) exhibit a transmission zero below the pass band, which provides a sharp cut-off. Additionally, the rejection level can be improved increasing the number of unit cells. Figure 17(b) shows the frequency response of a high pass filter formed by 3 unit cells like the one shown in Fig. 17(a) in which the achieved rejection level is 40dB at the stop band (Selga et al., 2009). In such kind of filters, the upper limit of the band is not controlled. However, if it is necessary, additional resonators can be included in the design in order to reject the signal at the desired frequency or even to create attenuation poles within the transmission band (Gil et al., 2007d).

Hybrid structures, on the other hand, exhibit a pass band response and there is no need to include additional resonators. Figure 17(c) and (d) show the layout and performance of an UWB band pass filter based on hybrid unit cells including CSRRs. The filter was designed to satisfy quite restrictive specifications, like -80dB rejection level at 2GHz, or a total size smaller than 1cm$^2$. The resulting device was formed by four identical unit cells implemented on a thin (0.127mm thickness) substrate with $\varepsilon_r$=10.2 and satisfied all imposed specifications, including the size limitation (Gil et al., 2007c). In Fig. 17(c), the dashed rectangle marks 1cm$^2$ area. As can be seen in Fig. 17(d), the filter is very selective, exhibits low insertion loss level at the pass band and a wide rejection band above the transmission band.

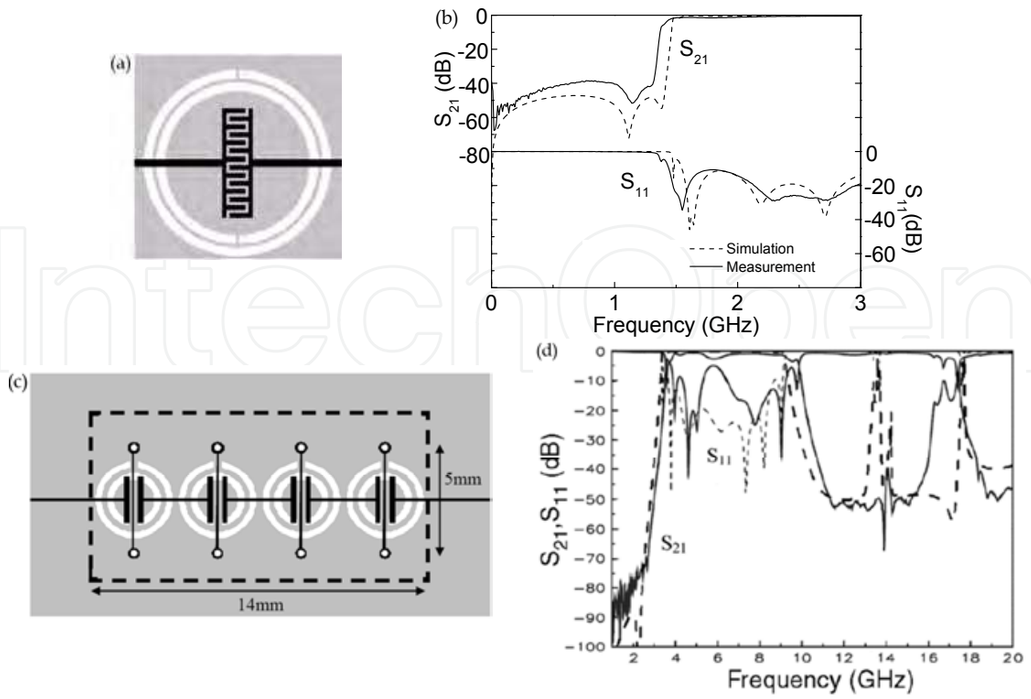


Fig. 17. (a) Layout of the balanced unit cell employed in the design of the high pass filter implemented in commercial substrate with $\varepsilon_r$=11 and thickness $h$=1.27mm. External radious of the resonators $r_{ext}$=4.17mm, ring width $c$=0.37mm, line width $w$=0.30mm, interdigital gap separation $g$=0.16mm. (b) Frequency response of high pass filter implemented by means of 3 unit cells like the one shown in (a). (c) Layout of a UWB band pass filter based on a balanced hybrid structure. Relevant dimensions are: line width $w$=0.126 mm, external radius of the resonator $r_{ext}$=1.68mm, ring width $c$=0.32mm and ring separation $d$=0.19 mm, inductor width is $w_l$=0.10mm and the gap distance $g$=0.4 mm (d) Simulated and measured frequency response of the filter shown in (c).

Other resonators can be employed to implement different kinds of filters, as is the case of OCSRRs. As has been previously mentioned, OCSRRs can be implemented in microstrip or coplanar technology. Figure 18 shows two examples of filters designed using these resonators. The filter in Fig. 18(a) is simply a low pass filter formed by 5 identical unit cells implemented with OCSRRs in microstrip technology (Aznar et al., 2009a). The design does not follow any standard approximation and a spurious band is present close to the cut-off frequency. In order to eliminate the first spurious band, a second stage formed by four unit cells is added to the low pass filter (Fig. 18(b)). As a result, the stop band is spurious free over a wider frequency range. Figure 18(c) includes the measured frequency responses of the two fabricated prototypes. As can be seen, a very sharp cut-off is obtained, as well as an important rejection level in the stop band, whereas insertion losses are very low in the pass band. Their frequency responses have been compared with the simulated response of a 0.5dB ripple elliptic filter with similar specifications, which must be an order 7 filter.

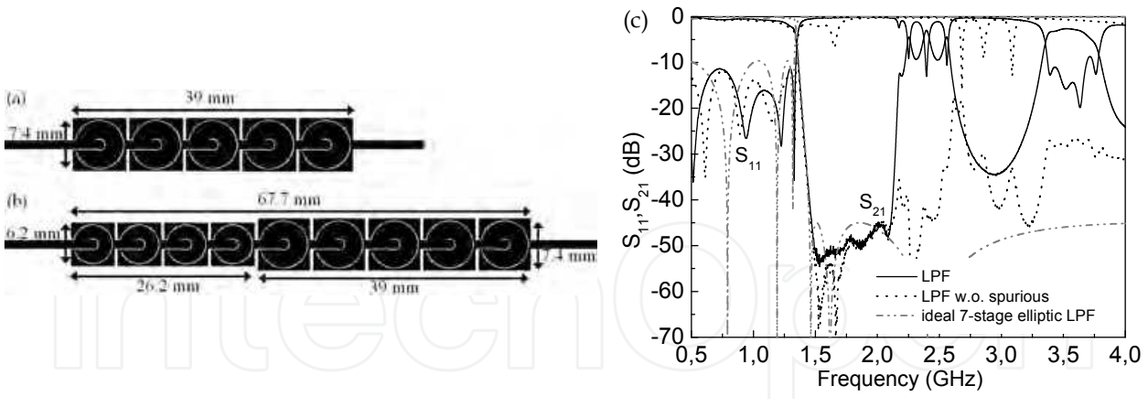


Fig. 18. (a) Layout of a microstrip low pass filter implemented with OCSRRs. The device was implemented in commercial substrate with $\varepsilon_r$=11 and $h$=1.27mm, the width of the gaps forming the OCSRRs is $c$=0.2mm, whereas $d$=2.46mm and $r_{ext}$=3.5mm. (b) Layout of a low pass filter including 4 OCSRRs for spurious with $c$=0.2mm, d=1.83mm, $r_{ext}$=2.9mm. (c) Measured responses of the filters (a) and (b) compared with the simulation of a 7-order elliptic filter.

Chebyshev filters can also be implemented by means of OCSRRs applying a similar methodology as the employed in the design of the filter shown in Fig. 16 (Vélez et al., 2009). This technique has been applied to the design of an order 5 filter with 0.1dB ripple, fractional bandwidth FBW=80% and central frequency $f_0$=5GHz. The resulting device can be observed in Fig. 19. Each section has been designed to satisfy the requirements to obtain the desired filter performance. This requires the implementation of the central unit cell by means of two resonators given that a smaller shunt inductance is required.

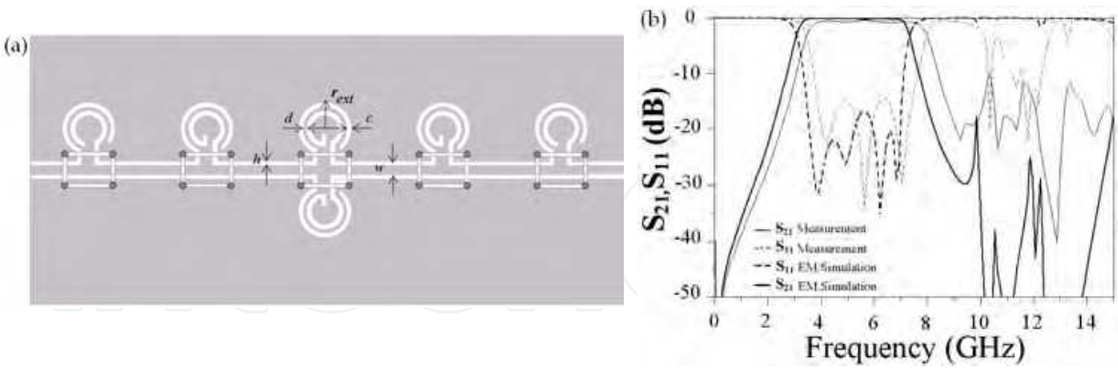


Fig. 19. (a) Layout of Chebyshev band pass filter based on OCSRRs implemented in coplanar waveguide technology. The device has been implemented in commercial substrate with $\varepsilon_r$=10.2 and 635μm thickness and $c$=0.22mm, $d$=0.15mm, $r_{ext}$=1.45mm, $w$=0.38mm, $h$=0.17mm.(b) Measured and simulated frequency response of the filter shown in (a).

The total length of the final device is 27mm, what corresponds to 0.9 times the wavelength of the signal at the central filter frequency. As can be seen, the filter exhibits good values of the insertion and return losses within the pass band. These two filters are some of the

application examples of OCSRRs for the implementation of microwave devices, which can be designed in coplanar and microstrip technologies.

## 5. Conclusion

In this chapter, different kinds of resonant-type metamaterial transmission lines based on subwavelength resonators have been presented and studied. There are several types of resonators which allow their use in the implementation of this kind of artificial transmission lines and their small size is exploited in order to achieve device miniaturisation. Besides their small size, metamaterial transmission lines allow the control of their electrical characteristics, opening the door to very competitive and innovative application possibilities. Among these applications, some microwave devices based on resonant-type metamaterial transmission lines have been shown. Power dividers, hybrid couplers and filters are some of the components which can be implemented by means of these transmission lines. The designed devices have compact dimensions and good performances, which are comparable to those of conventional devices. In some cases, there are some restrictions, like bandwidth, making such devices only suitable for narrow band applications. However, in other cases, the performance of conventional devices is even beaten by metamaterial devices. The manipulation of the dispersion diagram (also known as "dispersion engineering") is one of the tools that allows the improvement of certain performances or even to achieve new functionalities, like is the case of multi-band operation. Contrary to what occurs with conventional transmission lines, the use of metamaterial lines allows to choose arbitrary frequencies in multi-band applications. The manipulation and design of resonant-type metamaterial transmission lines requires equivalent circuit models providing a good description of the structures. These models have been presented, together with the parameter extraction methods that provide the circuit model parameters from the frequency response of the structure. These parameter extraction methods, besides being a very useful design tool, allow the corroboration of the proposed circuits as correct models for the corresponding structures. Work is in progress in the design of new devices based on the presented or new structures. New and more efficient design tools are being developed, as well as devices with new functionalities are being studied.

## 6. References

Alici, K. B.; Bilotti, F.; Vegni L. & Ozbay, E. Miniaturized negative permeability materials, *Applied Physics Letters*, vol. 91, August 2007, pp. 071121-3, ISSN 0003-6951.

Aznar, F.; Bonache, J. & Martín, F., Improved circuit model for left-handed lines loaded with split ring resonators, *Applied Physics Letters*, vol. 92, February 2008, pp. 043512-3, ISSN 0003-6951.

Aznar, F.; García-García, J.; Gil, M.; Bonache J. & Martín, F. Strategies for the miniaturization of metamaterial resonators, *Microwave and Optical Technology Letters*, vol. 50, May 2008, pp. 1263-1270, ISSN 1098-2760.

Aznar, F.; Gil, M.; Bonache, J. & Martín, Modelling metamaterial transmission lines: a review and recent developments, *Opto-Electronics Review*, vol. 16, September 2008, pp. 226-236, ISSN 1230-3402.

Aznar, F.; Gil, M.; Bonache, J.; Jelinek, L.; Baena, J. D.; Marqués, R. & F. Martín, Characterization of miniaturized metamaterial resonators coupled to planar transmission lines through parameter extraction, *Journal of Applied Physics*, Vol 104, December 2008, 114501, ISSN 0021-4922.

Aznar, F.; Vélez, A.; Bonache, J.; Menés J. & Martín, F. Compact lowpass filters with very sharp transition bands based on open complementary split ring resonators, *Electronics Letters*, Vol. 45, No. 6, March 2009, pp. 316-317, ISSN 0013-5194.

Aznar, F.; Gil, M.; Bonache, J. Valcarcel, A. & Martín, Miniaturization of narrow-band power dividers by using CPW metamaterial transmission lines, *Microwave and Optical Technology Letters*, Vol. 51, No. 4, April 2009, pp. 926-929, ISSN 0895-2477.

Baena, J. D.; Bonache, J.; Martín F.; Sillero, R. M.; Falcone, F.; Lopetegi, T.; Laso, M. A. G.; García-García, J.; Gil, I.; Portillo, M. F. & Sorolla, M. Equivalent-circuit models for split-ring resonators and complementary split-ring resonators coupled to planar transmission lines, *IEEE Transactions on Microwave Theory and Techniques*, vol. 53, April 2005, pp. 1451-1461, ISSN 0018-9480.

Bilotti, F.; Toscano, A.; Vegni, L.; Aydin, K.; Alici K. B. & Ozbay, E. Equivalent-circuit models for the design of metamaterials based on artificial magnetic inclusions, *IEEE Transactions on Microwave Theory and Techniques*, vol. 55, December 2007, pp. 2865-2873, ISSN 0018-9480.

Bonache, J.; Gil, I.; García-García, J. & Martín, F. Novel microstrip band pass filters based on complementary split rings resonators, *IEEE Transactions on Microwave Theory and Techniques*, vol. 54, January 2006, pp. 265-271, ISSN 0018-9480.

Bonache, J.; Gil, M.; Gil, I.; Garcia-García, J. & Martín, F., On the electrical characteristics of complementary metamaterial resonators, *IEEE Microwave and Wireless Components Letters*, vol. 16, October 2006, pp. 543.545, ISSN 1531-1309.

Bonache, J.; Sisó, G.; Gil, M.; Iniesta, A.; García-Rincón J. & Martín, F. Application of Composite Right/Left Handed (CRLH) Transmission Lines based on Complementary Split Ring Resonators (CSRRs) to the Design of Dual-Band Microwave Components, *IEEE Microwave and Wireless Components Letters*, Vol. 18 , Issue 8, August 2008, pp. 524-526, ISSN 1531-1309.

Caloz C. & Itoh, T. Application of the transmission line theory of left-handed (LH) materials to the realization of a microstrip "LH line", *Proceedings of IEEE Antennas and Propagation Society International Symposium,* vol. 2,pp. 412-415, ISBN 0-7803-7330-8, San Antonio, Texas, (USA), June 2002.

Caloz, C. & Itoh, T. (2005). *Electromagnetic Metamaterials: Transmission Line Theory and Microwave Applications*, Wiley Interscience, ISBN 978-0-471-66985-2.

Durán-Sindreu, M.; Aznar, F.; Vélez, A.; Bonache, J. & Martín, F. New composite, Right/Left handed transmission lines based on electrically small, open resonators, *Proceedings of IEEE MTT-S International Microwave Symposium*, pp. 45-48, ISBN 978-1-4244-2804-5, Boston (MA), USA, June 2009.

Eleftheriades, G. V.; Iyer A. K. & Kremer, P. C. Planar negative refractive index media using periodically L-C loaded transmission lines, *IEEE Transactions on Microwave Theory and Techniques*, vol. 50, December 2002, pp. 2702-2712, ISSN 0018-9480.

Eleftheriades, G. V. A Generalized Negative-Refractive-Index Transmission-Line (NRI-TL) Metamaterial for Dual-Band and Quad-Band Applications, *IEEE Microwave and Wireless Components Letters*, vol. 17, 2007, pp. 415-417, ISSN 1531-1309.

Falcone, F.; Lopetegi, T.; Laso, M. A. G.; Baena, J. D.; Bonache, J.; Beruete, M.; Marqués, R.; Martín, F. & Sorolla, M. Babinet principle applied to the design of metasurfaces and metamaterials, *Physical Review Letters*, vol. 93, November 2004, 197401, ISSN 1079-7114.

Gil, M.; Bonache, J.; Gil, I.; García-García, J. & Martín, F., On the transmission properties of left handed microstrip lines implemented by complementary split rings resonators, *Int. Journal Numerical Modelling: Electronic Networks, Devices and Fields*, vol. 19, March 2006 , pp 87-103, ISSN 0894-3370.

Gil, M.; Bonache, J.; Selga, J.; García-García, J. & Martín, F. Broadband resonant type metamaterial transmission lines, *IEEE Microwave and Wireless Components Letters*, vol. 17, February 2007, pp. 97-99, ISSN 1531-1309.

Gil, M.; Bonache, J.; Gil, I.; García-García, J. & Martín, F., Miniaturization of planar microwave circuits by using resonant-type left handed transmission lines, *IET Microwave Antennas and Propagation*, Vol.1, February 2007, pp. 73-79, ISSN 1751-8725.

Gil, M.; Bonache, J.; García-García, J.; Martel, J. & Martín, F. Composite right/left-handed metamaterial transmission lines based on complementary split-rings resonators and their applications to very wideband and compact filter design", *IEEE Transactions on Microwave Theory and Techniques*, Vol. 55, No. 6, June 2007, pp. 1296-1304, ISSN 0018-9480.

Gil, M.; Bonache, J. & Martín, F. Metamaterial filters with attenuation poles in the pass band for ultra wide band applications, *Microwave and Optical Technology Letters*, Vol. 49, Issue 12, December 2007, pp 2909-2913, ISSN 0895-2477. .

Gil, M.; Bonache, J. & Martín, F. Synthesis and applications of new left handed microstrip lines with complementary split-ring resonators etched on the signal strip, *IET Microwaves, Antennas & Propagation*, Vol. 2, Issue 4, June 2008 pp. 324 – 330, ISSN 1751-8725.

Gil, M.; Bonache, J. & Martín, F. Metamaterial Filters: A Review, *Metamaterials*, Vol. 2, Issue 4, December 2008, pp 186-197, ISSN 1873-1988.

Martel, J.; Marqués, R.; Falcone, F.; Baena, J. D.; Medina, F.; Martín F. & Sorolla, M. A new LC series element for compact bandpass filter design, *IEEE Microwave and Wireless Components Letters*, vol. 14, May 2004, pp. 210-212, ISSN 1531-1309.

Marqués, R.; Mesa, F.; Martel, J. & Medina, F. Comparative analysis of edge- and broadside-coupled split ring resonators for metamaterial design - Theory and experiments, *IEEE Transactions on Antennas and Propagation*, vol. 51, October 2003, pp. 2572-2581, ISSN 0018-926X.

Marqués, R.; Martín, F. & Sorolla, M. (2008). *Metamaterials with Negative Parameters*, John Wiley & Sons, Inc., ISBN 978-0-471-74582-2.

Martín, F.; Bonache, J.; Falcone, F.; Sorolla M. & Marqués, R. Split ring resonator-based left-handed coplanar waveguide, *Applied Physics Letters*, vol. 83, December 2003, pp. 4652-4654., ISSN 0003-6951.

Papanastasiou, A. C.; Georghiou, G. E. & Eleftheriades, G. V. A quad-band Wilkinson power divider using generalized NRI transmission lines, *IEEE Microwave and Wireless Components Letters*, vol. 18, August 2008, pp. 521-523, ISSN 1531-1309.

Schurig, D.; Mock, J. J.; Justice, B. J.; Cummer, S. A.; Pendry, J. B.; Starr A. F. & Smith, D. R. Metamaterial electromagnetic cloak at microwave frequencies, *Science*, vol. 314, 2006, pp. 977-980, ISSN 0036-8075.

Selga, J.; Aznar, F.; Vélez, A.; Gil, M.; Bonache, J. & Martín, F. Low-pass and high-pass microwave filters with transmission zero based on metamaterial concepts, *Proceedings of IEEE International Workshop on Antenna Technology (iWAT2009): Small Antennas and Novel Metamaterial*s, DOI 10.1109/IWAT.2009.4906914, March 2009, Santa Monica (CA), USA.

Sisó, G.; Bonache, J.; Gil, M.; García-García, J. & Martín, F, Compact rat-race hybrid coupler implemented through artificial left handed and right handed lines, *Proceedings of the IEEE MTT-S Int'l Microwave Symposium*, pp. 25-28, ISBN: 1-4244-0688-9, Honolulu, Hawaii (USA), June 2007.

Sisó, G.; Bonache, J. & Martín, F., Dual-Band Y-Junction Power Dividers Implemented Through Artificial Lines Based on Complementary Resonators, *Proceedings of the IEEE MTT-S Int'l Microwave Symposium*, pp. 663-666, ISBN: 978-1-4244-1780-3 Atlanta (USA), June 2008.

Sisó, G.; Bonache, J.; Gil, M. & Martín, F, Enhanced bandwidth and dual-band microwave components based on resonant-type metamaterial transmission lines, *International Journal of Microwave and Optical Technology*, Vol. 3, Issue 3, July 2008, pp. 345-352, ISSN 1553-0396.

Sisó, G.; Gil, M.; Aznar, F.; Bonache, J. & Martín, F. Generalized Model for Multiband Metamaterial Transmission Lines, *IEEE Microwave and Wireless Components Letters*, Vol. 18, Num. 11, November 2008, pp 728-730, ISSN 1531-1309.

Sisó, G.; Gil, M.; Aznar, F.; Bonache, J. & Martín, F. Dispersion engineering with resonant-type metamaterial transmission lines, *Laser & Photonics Review*, vol. 3, Issue 1-2, February 2009, pp. 12-29, ISSN 1863-8880.

Smith, D. R.; Padilla, W. J.; Vier, D. C.; Nemat-Nasser S. C. & Schultz, S. Composite medium with simultaneously negative permeability and permittivity, *Physical Review Letters*, vol. 84, May 2000, pp. 4184-4187, ISSN 0031-9007.

Vélez, A.; Aznar, F.; Bonache, J.; Velázquez-Ahumada, M. C.; Martel J. & Martín, F. Open complementary split ring resonators (OCSRRS) and their application to wideband cpw band pass filters, *IEEE Microwave and Wireless Components Letters*, vol. 19, April 2009, pp. 197-199, ISSN 1531-1309.

Vélez, A.; Bonache, J. & Martín, F. Metamaterial transmission lines with tunable phase and characteristic impedance based on complementary split ring resonators, *Microwave and Optical Technology Letters*, Vol. 51 Issue 8, August 2009, pp. 1966-1970, ISSN 0895-2477.

Veselago, V. G. The electrodynamics of substances with simultaneously negative values of ε and μ, *Soviet Physics Uspekhi*, January 1968, pp. 509-514, ISSN 0038-5670.

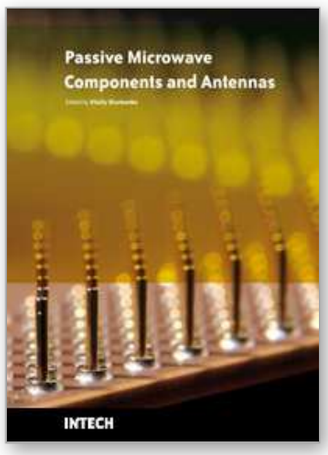


**Passive Microwave Components and Antennas**

Edited by Vitaliy Zhurbenko

ISBN 978-953-307-083-4
Hard cover, 556 pages
**Publisher** InTech
**Published online** 01, April, 2010
**Published in print edition** April, 2010

Modelling and computations in electromagnetics is a quite fast-growing research area. The recent interest in this field is caused by the increased demand for designing complex microwave components, modeling electromagnetic materials, and rapid increase in computational power for calculation of complex electromagnetic problems. The first part of this book is devoted to the advances in the analysis techniques such as method of moments, finite-difference time- domain method, boundary perturbation theory, Fourier analysis, mode-matching method, and analysis based on circuit theory. These techniques are considered with regard to several challenging technological applications such as those related to electrically large devices, scattering in layered structures, photonic crystals, and artificial materials. The second part of the book deals with waveguides, transmission lines and transitions. This includes microstrip lines (MSL), slot waveguides, substrate integrated waveguides (SIW), vertical transmission lines in multilayer media as well as MSL to SIW and MSL to slot line transitions.



**InTech Europe**
University Campus STeP Ri
Slavka Krautzeka 83/A
51000 Rijeka, Croatia
Phone: +385 (51) 770 447
Fax: +385 (51) 686 166
www.intechopen.com

**InTech China**
Unit 405, Office Block, Hotel Equatorial Shanghai
No.65, Yan An Road (West), Shanghai, 200040, China
中国上海市延安西路65号上海国际贵都大饭店办公楼405单元
Phone: +86-21-62489820
Fax: +86-21-62489821

IntechOpen